THE DESIGN OF A PRECISION MECHANICAL ASSEMBLY FOR A HARD X-RAY POLARIZER

S. P. Kearney, D. Shu, T. S. Toellner

Advanced Photon Source, Argonne National Laboratory, Argonne, IL 60439, U.S.A.

Abstract

This paper discusses the mechanical design of an x-ray polarizer and the analysis of the design using FEA simulation. In addition, insight was made into the meshing requirements of flexure mechanisms. It was found that the maximum flexure stress will increase in accuracy with a finer mesh, however there is a limit to how well FEA can model stiffness and deflection without incorporating additional advanced FEA analysis techniques such as nonlinear methods. Finally, it was shown that the pitch stages for the polarizer will be capable of a least 80 nrad resolution.

INTRODUCTION

A hard x-ray polarizer is under development for the Advanced Photon Source (APS) at Argonne National Laboratory (ANL). It has been previously shown that polarization of synchrotron radiation can be used to filter a narrow bandwidth of 14.4 keV [1]. This has advantages for Mossbauer spectroscopy (MS) in that it allows for energy spectra to be collected rather than time spectra, which is normal in synchrotron radiation [2].

The paper will first detail and describe the mechanical design of the polarizer device for hard x-rays. Particular attention is paid to the analysis of the flexure mechanism involved in nano-radian level rotations. FEA simulations of a single notch type flexure are conducted followed by simulation of the complete flexure mechanism. Finally, experimental resolution results are shown.

POLARIZER DESIGN

Assembly – Z8-4600

The complete polarizer assembly consists of a total of 7 degrees of freedom (DOF). Three crystals are manipulated using individual actuator stacks, as can be seen in Fig. Figure 1. The left crystal will sit atop two Kohzu™ ST05A-S1T-R tilt stages modified to incorporate Newport™ 8301NF Picomotors™ for controlled positioning in the yaw and roll angles. The middle crystal also has two DOF with the base stage being a custom-designed high precision pitch flexure stage (Z4-4601) and atop that a Kohzu™ ST07A-S1T yaw tilt stage, which also incorporates a slightly larger 8302 Picomotor™ for controlled positioning. Finally, the third crystal has three DOF with the base stage being a more compact version of Z4-4601 designated Z4-4602. Atop this stage is a translation stage Kohzu™ XM05A-C1-R, and another ST05A-S1T-R roll tilt stage with Picomotor™ 8301NF. The detailed design specifications for the assembly can be seen in Table 1.

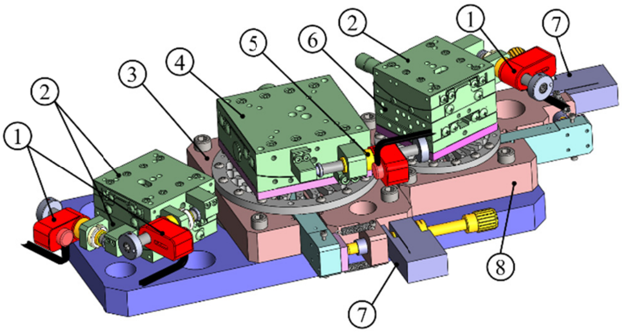

Figure 1: Z8-4600 assembly model view. Numbered items are 1) 3X Picomotor™ 8301NF, 2) 3X Kohzu™ ST05A-S1T-R tilt stage, 3) Z8-4601 pitch stage, 4) Kohzu™ ST07A-S1T tilt stage, 5) Picomotor™ 8302, 6) Kohzu™ XM05A-C1-R translation stage, 7) 2X Newport™ NPM140SG micrometer adapter piezo, and 8) Z8-4602 pitch stage.

Table 1: Design specifications for Z8-4600. The resolutions listed are derived from the published resolutions of the commercial actuators and represent the lower limit.

Specification	Value
Volume (L x W x H) mm^3	(365x214x89)
Mass	4.1 kg
Degrees of Freedom	7
Kohzu™ Tilt Stages Resolution	
ST05A-S1T-R (Open Loop)	0.5 µrad
ST07A-S1T(Open Loop)	0.4 µrad
Kohzu™ Stages Range	
ST05A-S1T-R & ST07A-S1T	±3°
XM05A-C1-R	±3.25 mm
Pitch Flexure Stages Resolution	
Z4-4601 & Z4-4602 (Closed Loop)	15 nrad
Pitch Flexure Stages Range	
Z4-4601 & Z4-4602	±0.7°

Pitch Rotation Stage – Z8-4602

Two laminar weak-link stages have been designed, for fine pitch rotation. For this paper, we will focus on the smaller diameter (73.34 mm vs. 97.78 mm) flexure stage shown in Fig. Figure 2. Pitch rotation is achieved by a Newport™ NPM140SG actuator pushing on an 80 mm sine bar attached to a pair of weak-link flexures. The laminar weak-link structure is comprised of 30 bonded sheets of 17-7 PH stainless steel 0.1524 mm thick each [3-5].

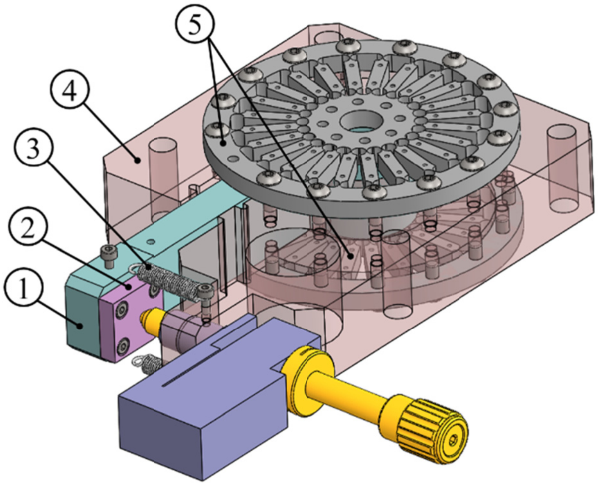

Figure 2: Z8-4602 sub-assembly model view. Numbered items are 1) 80 mm sine bar, 2) 440 hardened SS contact plate, 3) 2X extension springs, 4) base plate (shown transparent for clarity), 5) 2X 73.34 mm diameter weak-link flexure.

As of publication only the Z8-4602 stage has been built and is used as the base prototype for FEA simulation validation and experimentation. The results of these studies have provided insight into the development of Z8-4601 and similar stages based on this design.

DESIGN ANALYSIS

Flexure Modelling

The principal component of the Z4-4602 precision pitch stage is a flexure mechanism. To better understand this larger flexure mechanism, we will first analyze a single notch type flexure.

Figure 3 shows a single notch type flexure on the left with its coordinates and critical dimensions used in analytical models. The critical dimensions are R the notch radius, t flexure thickness, and b flexure depth.

By integrating the beam equation with strip elements of the flexure an approximation of the torsional stiffness about θ_Y is given by

$$K_{\theta_Y} = \frac{M}{\theta_Y} = \frac{2EbR^2}{3f(\beta)}, with \tag{1}$$

$$f(\beta) = \frac{1}{\Delta}\left\{\left(\frac{3+4\beta+2\beta^2}{\gamma\Delta}\right) + \left(\frac{6\gamma}{\Delta^{3/2}}\right)\tan^{-1}\sqrt{\frac{2+\beta}{\beta}}\right\},$$

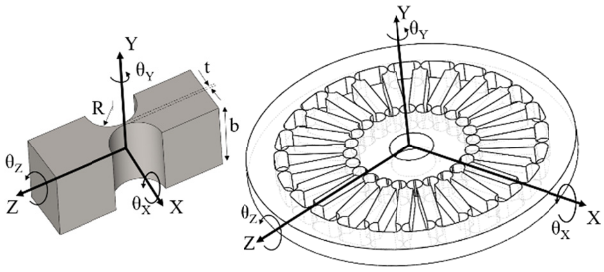

Figure 3: Coordinate frames for the two FEA models used in this study. On the left is a single flexure with dimensions describing b depth, t flexure thickness, and R semi-circular notch radius. On the right is the complete laminar weak-link structure with the coordinate frame now located at the center of the pitch pivot axis, θ_Y.

and with $\beta =$ t/(2R), $\gamma = 1 + \beta$, $\Delta = 2\beta + \beta^2$, E the Young's modulus, and M the applied bending moment [6]. Equation (1) is an approximation, and it has a further simplification given by

$$K_{\theta_Y} = \frac{M}{\theta_Y} = \frac{2Ebt^{5/2}}{9\pi R^{1/2}}. \tag{2}$$

The nominal stress can then be determined from the equation

$$\sigma_{nom} = \frac{6M}{t^2 b}. \tag{3}$$

However, it should be noted that this assumes constant cross section and does not account for the concentration of stress that comes from a sudden change in cross-sectional geometry. C. B. Ling [7] derived the exact solution for this stress and it can be determined from the nominal stress using a stress concentration factor K_t

$$\sigma = K_t \sigma_{nom}. \tag{4}$$

The stress concentration factor can be determined graphically using the chart in [8] or from [6] using

$$K_t = (1+\beta)^{9/20} \tag{5}$$

For this paper we will refer to calculations using Eqs. (1), (4), and (5) as Ling's method and Eqs. (2) and (3) as the approximate method.

For the Z4-4602 flexure design stress, angle, and torsional stiffness are calculated using t = 0.115 mm, b = 4.752 mm, R = 1.524 mm, E = 204 GPa, and M = 1 N·mm. These calculations for both analytical methods can be seen in Table 2. The error from using the approximate method is at most 2.7 % for this case. Considering that there is no substantially greater numerical effort required to use Ling's method as compared to the approximate method there is no reason not to use the more complete Ling method. Therefore, Ling's method is be used in this paper to assess FEA model validity.

Table 2: Comparing theoretical methods for calculation of stress, angle of rotation, and stiffness of the notch flexure.

Method	Stress [Mpa]	Angle [°]	Torsional Stiffness [N·mm/°]
Ling's	100.9	0.25	4.07
Approx.	99.2	0.24	4.18
% Error	-1.65	-2.68	2.70

FEA Flexure Mesh Validation

To ensure that the larger flexure FEA model is meshed with an adequate number of elements so that there can be confidence in the results, we first validate the single notch flexure mesh. We do this using a method described in a previous MEDSI 2014 conference paper [9]. For a single notch flexure, the mesh will be increased in density using SolidWorks Simulation 2016 h-adaptive mesh refining loops. The results are then compared to theoretical calculations.

The FEA mesh and setup can be seen in Figure 4 with the same geometry, material, and moment properties used in the previous section. The mesh shown is that for 5 adaptive mesh loops. At this mesh size there are at least 2 elements across the thinnest part of the flexure. Next to the setup is the von Mises stress results. In the close up of the stress results a sudden spike in stress can be seen only near the surface. This is the stress concentration that needs to be captured for the FEA model to be valid. So, the elements near the surface are much more critical than those within the volume.

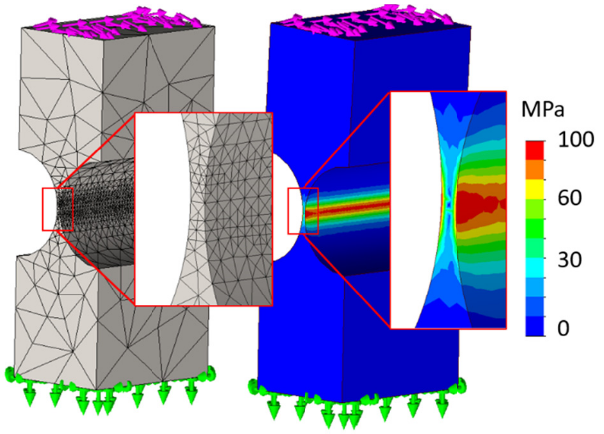

Figure 4: Setup and results of the 5 loops case. On the left is the FEA setup of the single flexure model. The green arrows on the bottom represent the fixed condition and the magenta arrows on the top represent the pure bending moment about the axis θ_Y. On the right is the von Mises stress results with an exaggerated deformation shown.

The results of the setup in Figure 4 are low in error, especially for the max stress criteria, as can be seen in the plot of Figure 5. Here, the error of the FEA results compared to theory is shown as the number of mesh loops is increased. Interestingly, as the mesh density increases (increasing mesh loops) the error in rotation angle and torsional stiffness becomes constant, while the maximum stress error continues to decrease. From the plot we can also see that a mesh using 4 or 5 loops will reduce stiffness and angle errors as far as they will go, and the max stress errors will be around 5%. For the larger flexure model we then used 5 adaptive mesh loops.

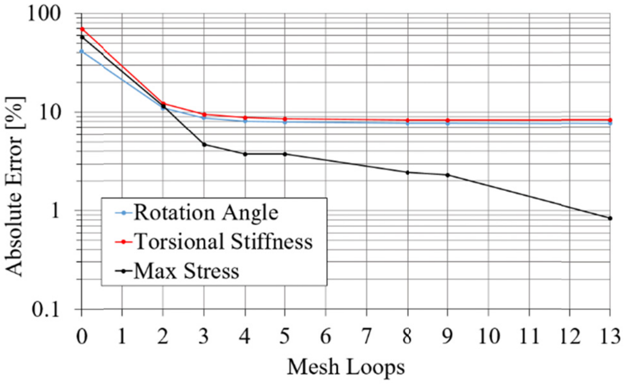

Figure 5: A plot of the relationship between adaptive mesh loops and the absolute error of the FEA model parameters: rotation angle, torsional stiffness, and max stress compared to theoretical predictions.

FEA Weak-Link Model Validation and Simulation

Now using the 5 h-adaptive mesh loops to reduce the stress error to about 5%, as shown in the previous section the full flexure model will be implemented, Figure 6. We first validate the quality of the FEA model by comparing the derived stiffness values to experimentally measured stiffness, and then predict the load capacity of the flexure stage.

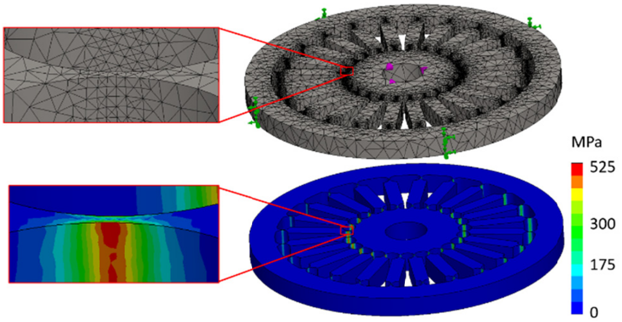

Figure 6: Setup and results using 5 adaptive mesh loops and 0.5 (N·m) of torque applied about the θ_Y axis. On the top is the FEA setup with green arrows on the outside axis representing the fixed condition and the magenta arrows on the inside hole diameter representing the applied torque. On the bottom is the von Mises stress results with about 0.6° rotation about θ_Y.

For stiffness validation the flexure model torsional stiffness is measured and then converted to an equivalent linear spring stiffness that is equivalent to the stiffness measured using the setup in Figure 7. Figure 8 shows the results of the stiffness validation. Here we can see that the two force gauge lines overlap, which demonstrates the reliability of the experimentally measured stiffness. Looking at the FEA stiffness results it can be seen that a good match between model and experiment only occurs up to about ~300 µm of equivalent actuator travel. There are many reasons why the FEA model might not be valid past this range; such as the real structure is a bonded stack of 30 laminar sheets of metal, the FEA analysis is linear, and tolerance variations in the real flexure thickness are not accounted for. In future studies these issues will be addressed.

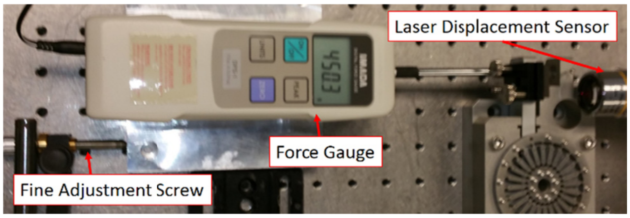

Figure 7: Experimental setup of stiffness measurement for the Z4-4602 sub-assembly.

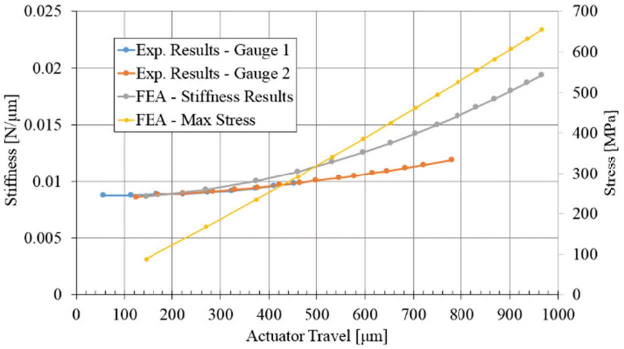

Figure 8: A plot of the stiffness of the Z4-4602 sub-assembly experimentally measured with two force gauges of different precision, gauge 1 being the finer precision of ± 0.001 N and gauge 2 with a precision of ± 0.01 N. Also plotted is the stiffness acquired from the FEA model and the max stress. Note the model can only be validated for use from 0 to ~300 µm of equivalent actuator travel.

Lastly, the model is used inside of the validated region to assess the effect of loading the flexure in the Y direction. An equivalent load of 2 kg was placed on the inside diameter of the flexure and an equivalent moment that would be applied due to a 270 µm actuator displacement. The resulting maximum von Mises stress is 171 MPa and caused 0.63 µm of parasitic motion in the Y direction. This is equivalent to a stiffness in the Y direction of 31.3 N/µm, three orders of magnitude greater than the pitch rotation direction.

Z4-4602 EXPERIMENTAL RESULTS

The fine positioning resolution was tested using a PI™ P840.10 piezo due to unavailability of the NPM140SG actuator. The P840.10 has a stated closed loop resolution of 1 nm. The experimental setup can be seen in Figure 9. Displacement was measured using a Polytec™ OFV 534 vibrometer. Figure 10 shows a set of ~80 nrad steps. The noise floor of the setup looks to be about 20 nrad which is mostly contributed by the P840.10 closed loop control. If we disregard slow drifting, the noise floor of the setup with P840.10 open loop control is about 5 – 10 nrad.

CONCLUSION

Design and development of a mechanism for a hard x-ray polarizer was assessed using FEA simulation and experiment. It was found that the maximum flexure stress will increase in accuracy with a finer mesh, however there is a limit to how well FEA can model stiffness and deflection without incorporating additional advanced model techniques such as nonlinear methods. Finally, it was shown that pitch stages for the polarizer will be capable of a least 80 nrad resolution.

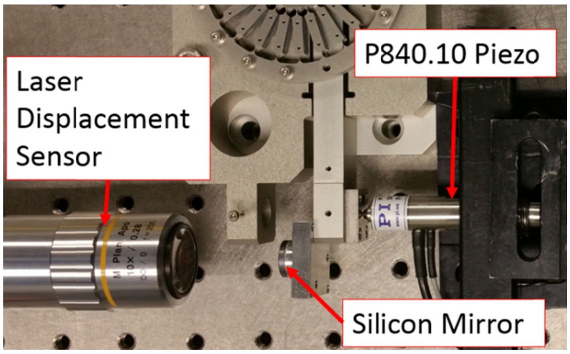

Figure 9: Experimental setup to measure the pitch angle. In this setup an alternative actuator is used to analyze the ultimate capabilities of the stage design.

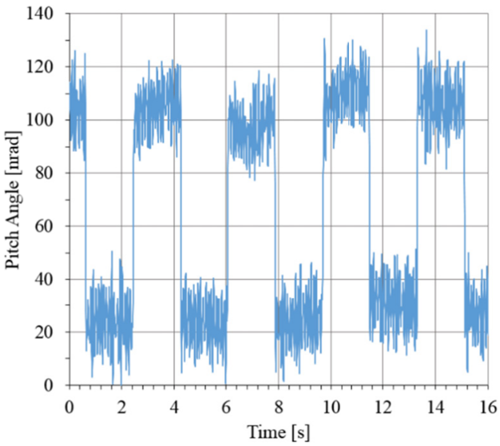

Figure 10: A plot of ~80 nrad steps.

ACKNOWLEDGMENT

Work supported by the U.S. Department of Energy, Office of Science, under Contract No. DE-AC02-06CH11357.

REFERENCES

[1] T. Toellner *et al.*, "Polarizer/analyzer filter for nuclear resonant scattering of synchrotron radiation," *Applied physics letters,* vol. 67, no. 14, pp. 1993-1995, 1995.

[2] T. S. Toellner, A. Alatas, E. E. Alp, M. Hu, and J. Zhao, "Next-Generation Mossbauer Spectroscopy," Argonne National Laboratory, 2015-164-N0, 2015.

[3] D. Shu, T. S. Toellner, and E. E. Alp, "Redundantly constrained laminar structure as weak-link mechanisms," U.S. Patent granted No. 6,607,840, 2003

[4] D. Shu, T. S. Toellner, and E. E. Alp, "Redundantly constrained laminar structure as weak-link mechanisms," U.S. Patent granted No. 6,984,335, 2006

[5] D. Shu, S. Narayanan, A. Sandy, M. Sprung, C. Preissner, and J. Sullivan, "Precision mechanical design of an UHV-compatible artificial channel-cut x-ray monochromator," AIP CP879, pp. 1073-1076 (2007).

[6] S. T. Smith, V. G. Badami, J. S. Dale, and Y. Xu, "Elliptical flexure hinges," *Review of Scientific Instruments,* vol. 68, no. 3, pp. 1474-1483, 1997.

[7] C.-B. Ling, "On the stresses in a notched strip," *J. of Appl. Mech. Trans. ASME*, vol. 19, no. 2, pp. 141-146, 1952.

[8] R. Peterson, "Stress concentration factors, 1974," *John Willey and Sons*

[9] M. Hillman, "Design of a flexural hinge mechanism for turbo slits," in *Proc. MEDSI '14*, Melbourne, Australia, 2014.